Biochimica et Biophysica Acta 1848 (2015) 1005–1013

Contents lists available at ScienceDirect

Biochimica et Biophysica Acta

journal homepage: www.elsevier.com/locate/bbamem

Multiple effects of anthracene-9-carboxylic acid on the TMEM16B/anoctamin2 calcium-activated chloride channel

O. Lijo Cherian [a], Anna Menini [a], Anna Boccaccio [b,*]

[a] Neurobiology Group, SISSA, International School for Advanced Studies, Via Bonomea 265, 34136 Trieste, Italy
[b] Istituto di Biofisica, CNR, Via De Marini 6, 16149 Genova, Italy

ARTICLE INFO

Article history:
Received 29 October 2014
Received in revised form 4 January 2015
Accepted 13 January 2015
Available online 22 January 2015

Keywords:
Ca^{2+}-activated Cl^- channel
Patch clamp
ANO2
Blocker
A9M
A9C

ABSTRACT

Ca^{2+}-activated Cl^- currents (CaCCs) play important roles in many physiological processes. Recent studies have shown that TMEM16A/anoctamin1 and TMEM16B/anoctamin2 constitute CaCCs in several cell types. Here we have investigated for the first time the extracellular effects of the Cl^- channel blocker anthracene-9-carboxylic acid (A9C) and of its non-charged analogue anthracene-9-methanol (A9M) on TMEM16B expressed in HEK 293T cells, using the whole-cell patch-clamp technique. A9C caused a voltage-dependent block of outward currents and inhibited a larger fraction of the current as depolarization increased, whereas the non-charged A9M produced a small, not voltage dependent block of outward currents. A similar voltage-dependent block by A9C was measured both when TMEM16B was activated by 1.5 and 13 μM Ca^{2+}. However, in the presence of 1.5 μM Ca^{2+} (but not in 13 μM Ca^{2+}), A9C also induced a strong potentiation of tail currents measured at −100 mV after depolarizing voltages, as well as a prolongation of the deactivation kinetics. On the contrary, A9M did not produce potentiation of tail currents, showing that the negative charge is required for potentiation. Our results provide the first evidence that A9C has multiple effects on TMEM16B and that the negative charge of A9C is necessary both for voltage-dependent block and for potentiation. Future studies are required to identify the molecular mechanisms underlying these complex effects of A9C on TMEM16B. Understanding these mechanisms will contribute to the elucidation of the structure and functional properties of TMEM16B channels.

1. Introduction

Ca^{2+}-activated Cl^- currents (CaCCs) were originally identified in rod segments from the salamander retina [1] and in *Xenopus laevis* oocytes [2]. Later they have been observed in diverse tissues including exocrine gland cells, neurons, heart, skeletal and smooth muscle [3–12].

The molecular identity of CaCCs has been controversial for a long time, until recently, when two members of TMEM16/anoctamin gene family, TMEM16A/anoctamin1 and TMEM16B/anoctamin2, were shown to mediate CaCCs [13–21].

TMEM16A and TMEM16B were found to be expressed in many of the cell types known to exhibit CaCCs [12,21–23]. Studies performed with knockout mice for TMEM16A or TMEM16B [24,25] and knockdown of these channels in specific cell types confirmed their involvement in the generation of CaCCs [12,26–32].

TMEM16A and TMEM16B are closely related [21] and their expression in diverse cell types gives rise to CaCCs with some different properties: TMEM16B shows faster kinetics and lower sensitivity to cytosolic Ca^{2+} than TMEM16A [13–17,33].

Diverse classes of compounds were reported to block CaCCs in various cell types, like fenamates (flufenamic acid, niflumic acid) [34–36], stilbene derivatives (4,4-diisothiocyanato-stilbene-2,2-disulfonic acid, known as DIDS) [37] and anthracene-9-carboxylic acid (A9C; [37]). Unfortunately, these compounds lack specificity and high affinity. Other blockers, such as eugenol [38], digallic and tannic acids [39], benzbromarone [40], $CaCC_{inh}$-A01 [41] and the novel $T16A_{inh}$-A01 [42] and MONNA [43], have been identified recently. The investigation of their specificity and blocking mode is still in progress.

Anthracene-9-carboxylic acid (A9C) is an organic molecule traditionally used to block and identify CaCCs in various cell types, like diverse smooth muscle cells (from portal vein [37,44]; esophageal [45]; urethral [46]; anococcygeal [47] and lymphatic smooth muscle cells [48]), but also in epithelial cells [49], in salivary gland cells [50] and in *X. laevis* oocytes [51].

A9C has been described as a low-affinity open channel voltage-dependent blocker of CaCCs measured in excised patches from *X. laevis* oocytes, blocking the current at depolarizing voltages and acting from the extracellular side [51].

* Corresponding author at: Istituto di Biofisica — IBF, Consiglio Nazionale delle Ricerche — CNR, Via De Marini 6, 16149 Genova, Italy. Tel.: +39 010 6475 891; fax: +39 010 6475500.
E-mail address: boccaccio@ge.ibf.cnr.it (A. Boccaccio).

http://dx.doi.org/10.1016/j.bbamem.2015.01.009
0005-2736/

Piper and Greenwood [52] observed an anomalous and more complex action of A9C on CaCCs recorded in rabbit pulmonary artery smooth muscle cells, consisting of a weak block of outward currents and an increase of the amplitude of instantaneous inward currents recorded at hyperpolarizing potentials after a depolarizing prepulse.

In this study, we used the analysis of the blocking mechanisms of TMEM16B current by A9C as a method to contribute to the understanding of the structure, functional properties and action mechanisms of TMEM16B channels. We investigated the effect of extracellular A9C on TMEM16B Ca^{2+}-activated Cl^- currents, recorded in HEK 293T cells using the whole-cell patch-clamp technique. We activated TMEM16B including in the pipette solution either 13 μM Ca^{2+}, a concentration producing an almost full activation of TMEM16B-mediated current, or 1.5 μM Ca^{2+}, a sub-saturating Ca^{2+} concentration. In the presence of 13 μM Ca^{2+}, 1 mM A9C caused a voltage-dependent block of outward TMEM16B-mediated currents. However, when channels were activated by 1.5 μM Ca^{2+}, A9C showed multiple effects: a voltage-dependent block of outward currents, a strong potentiation of transient early inward currents, as well as potentiation of tail currents at −100 mV. We also tested the effect of anthracene-9-methanol (A9M), a non-charged analogue of A9C, and found that A9M produced a small not voltage-dependent block and did not cause current potentiation, indicating that the negative charge of A9C is involved in these effects.

2. Materials and methods

2.1. Cell culture and heterologous expression of TMEM16B

The full length isoform of TMEM16B cDNA in pCMV-Sport6 mammalian expression plasmid was obtained from RZPD (clone identification IRAV p968H1167D; NCBI protein database accession number NP_705817.1). This is the retinal isoform with the same start site of the olfactory isoform used by Stephan et al. [17] and contained the exon 14 [53], named exon 13 in [17]. 2 μg cDNA coding for TMEM16B together with 0.2 μg of pEGFP-C1 (Takara Bio Inc.) was transfected into HEK293T cells using FuGENE 6 or X-tremeGENE 9 (Roche). Cells were used for patch clamp experiments within 48 h of transfection.

2.2. Electrophysiology

Experiments were performed in the whole-cell voltage-clamp configuration at room temperature (22–25 °C). Patch pipettes, made of borosilicate glass had a pipette resistance of ~3–5 MΩ when immersed in bath solution. Whole cell currents were recorded with an Axopatch 1D amplifier controlled by pClamp 9.2 via a Digidata 1332A (Axon Instruments or Molecular Devices). Data were low pass filtered at 5 kHz and sampled at 10 kHz. Stimulation protocols consisted of voltage steps of 200 ms duration from a holding potential of 0 mV (or −60 mV) ranging from −100 mV to +140 mV with an interval of 20 mV, followed by a step to −100 mV.

2.3. Solutions

The standard extracellular solutions (mammalian Ringer) contained (in mM): 140 NaCl, 5 KCl, 2 $CaCl_2$, 1 $MgCl_2$, 10 glucose and 10 HEPES adjusted to pH 7.4 with NaOH. The standard intracellular solutions contained (in mM): 140 CsCl, 10 HEPES, 10 HEDTA, adjusted to pH 7.2 with CsOH, and various amounts of $CaCl_2$, as calculated with the program WinMAXC (C. Patton, Stanford University, Stanford, CA), to obtain free Ca^{2+} concentrations of 1.5 and 13 μM [54]. Anthracene-9-carboxylic acid, A9C, was dissolved in DMSO at a stock concentration of 1 M and stored at −20 °C. Final concentrations of A9C were achieved by diluting the desired volume of stock into bath solution and sonicating for 30 min at 37 °C. Anthracene-9-methanol, A9M, was dissolved in chloroform at a concentration of 100 mM and diluted in bath solution to a final concentration of 300 μM. The solution was sonicated until it became clear and was left open under chemical hood to evaporate the remaining chloroform. The maximal nominal concentration of chloroform in the final solution was 0.3%. All the preparations and experiments with A9C and A9M were done in dim light to minimize solutions' light exposure. All the chemicals were purchased from Sigma-Aldrich.

Different extracellular solutions were applied using a gravity fed multibarrel perfusion system consisting of three square glass pipes of 1 mm diameter through which different solutions could flow (Perfusion Fast Step SF-77B, Warner Instruments Corp.). Exchange of solutions around the patched cell was achieved by positioning one of the glass pipes, in which the test solution was flowing, in front of the cell. Bath was grounded using a 3 M KCl agar salt bridge connected to an Ag/AgCl reference electrode. Liquid junction potentials were of few mV and were not corrected.

2.4. Data analysis

Data analysis and figures were made using IGOR Pro software (WaveMetrics, Lake Oswego, OR, USA). Data are usually presented as mean ± SEM and the number of cells (n). Statistical significance was determined using paired or unpaired t tests, or ANOVA, as appropriate. When a statistically significant difference was determined with ANOVA, a post-hoc Tukey's test was done to evaluate which data groups showed significant differences. P values < 0.05 were considered significant.

For the sake of clarity in the figures the capacitive transients of some traces were trimmed.

3. Results

3.1. Voltage-dependent A9C block of TMEM16B currents

To measure the extracellular effect of A9C on TMEM16B-mediated currents, we recorded from HEK293T cells transiently transfected with TMEM16B using the whole-cell patch-clamp configuration in the presence of 1.5 or 13 μM free Ca^{2+} in the intracellular solution. Control experiments were performed in mock transfected cells and the average current in the presence of 1.5 ($n = 12$) or 13 μM ($n = 11$) free Ca^{2+} in the intracellular solution was respectively −10 ± 2 pA and −135 ± 55 pA at −100 mV and 142 ± 29 pA and 385 ± 133 at +100 mV.

In the first set of experiments, currents were activated by 13 μM Ca^{2+}, a concentration that has been previously reported to produce an almost full activation of TMEM16B-induced currents [16,17,55,56]. Fig. 1A shows representative whole-cell recordings measured in control and in the presence of 1 mM A9C, obtained in response to voltage steps between −100 and +140 mV, from a holding potential of 0 mV, followed by a step to −100 mV. I–V relations at the end of voltage steps show that outward currents were partially reduced by A9C (Fig. 1B). The average ratios between current in A9C and control (I_{A9C}/I_{CT}) plotted versus voltage reveal that the block was voltage-dependent and that A9C inhibited a larger fraction of the current when depolarization increased (Fig. 1C). A9C application to mock transfected cell had no effect (data not shown).

3.2. Multiple effects of A9C

In the second set of experiments, we reduced channel activation by decreasing intracellular Ca^{2+} to 1.5 μM, a concentration at which about 50% of the maximal TMEM16B-induced current is activated at +100 mV (Fig. 4A in [55]). Fig. 2A shows that, when the holding potential was 0 mV, addition of 1 mM A9C produced not only a voltage-dependent block of outward currents, as observed with 13 μM Ca^{2+} (Fig. 1), but also a transient increase of early inward currents recorded at hyperpolarizing voltages.

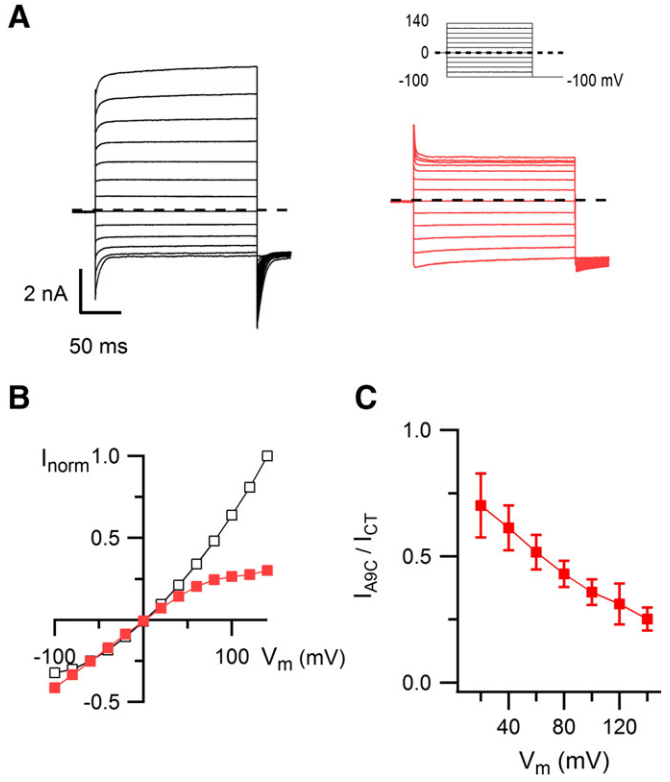

Fig. 1. Voltage dependence of A9C block in 13 μM Ca^{2+}. (A) Whole-cell currents recorded in the presence of 13 μM intracellular Ca^{2+}, with voltage steps from −100 to +140 mV from a holding potential of 0 mV in control (black) or in the presence of 1 mM A9C (red). Stimulation protocol is shown in top right side. (B) I–V relations measured at the end of the voltage steps from the cell shown in A normalized to the control value at +140 mV. (C) Average fractional current as a function of voltage (n = 4).

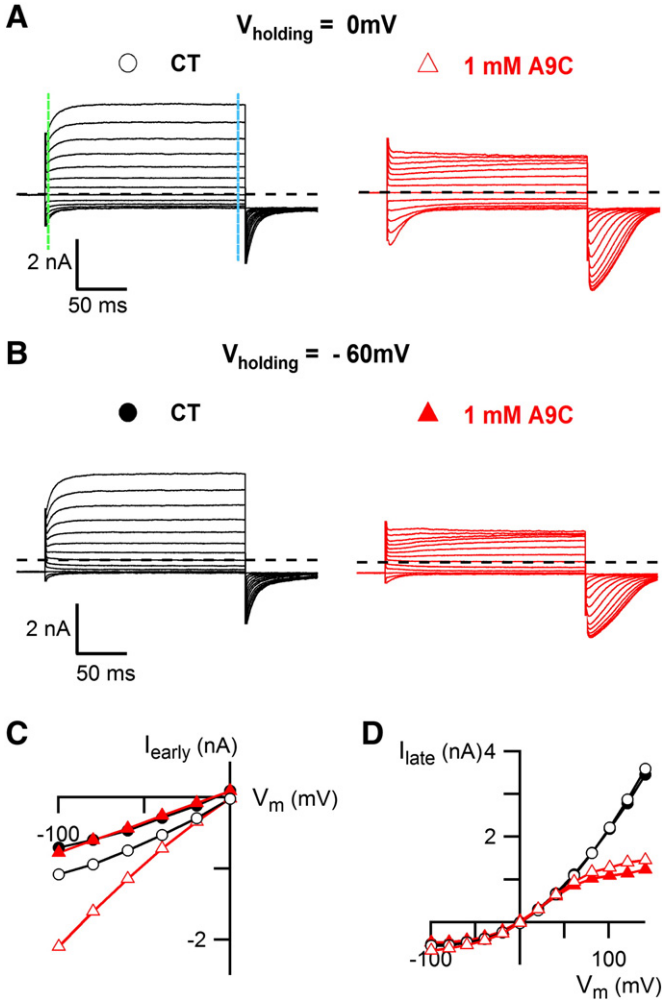

Fig. 2. Holding potential affects early inward current potentiation. Whole-cell currents recorded in the same cell in the presence of 1.5 μM intracellular Ca^{2+}, with voltage steps from −100 to +140 mV from a holding potential ($V_{holding}$) of 0 mV (A) or −60 mV (B), in control (black) or in 1 mM A9C (red). (C) I–V relations from −100 to 0 mV of early peak inward currents evaluated at the time indicated by the green vertical line for the cell shown in A, B. Peak inward currents were strongly potentiated in A9C when $V_{holding}$ was 0, but not −60 mV. (D) I–V relations at the end of the voltage steps (at the time of the blue vertical line) for experiments shown in A and B.

Fig. 2B shows currents recorded from the same cell as in A, from a holding potential of −60 mV. In the presence of 1 mM A9C, the amplitude of transient early inward currents did not change compared to control (Fig. 2C), whereas the voltage-dependent block of outward currents was similar to that measured from a holding potential of 0 mV (Fig. 2A, B and D). Similar results were obtained in 5 cells, in which currents were recorded at a holding potential of both 0 and −60 mV.

In addition, in 1.5 μM Ca^{2+}, we observed a strong potentiation of tail currents measured at −100 mV after depolarizing voltages (Fig. 2A and B), as we will describe in more detail in a subsequent section.

These results show that 1 mM A9C has multiple effects on TMEM16B in the presence of 1.5 μM Ca^{2+}, consisting of a voltage-dependent block of outward currents, and potentiation of tail currents measured at −100 mV after depolarizing voltages. In addition, early inward current potentiation was elicited by 1 mM A9C from a holding potential of 0 mV, whereas no potentiation was observed from a holding potential of −60 mV.

Fig. 3A shows that, in the presence of 1.5 μM Ca^{2+}, the kinetics of deactivation of tail currents recorded at −100 mV after several prepulse voltages could be well described by a single exponential function in control, whereas the deactivation kinetics in the presence of 1 mM A9C was complex. To quantify tail current potentiation after each prepulse voltage, we evaluated the maximal tail currents with respect to the values measured at steady state at −100 mV. In control, we calculated the current value obtained from a single-exponential fit of tail currents extrapolated to the beginning of the step to −100 mV (Fig. 3B, exponential fit in gray). In the presence of A9C, we measured the current peak that developed between 2.5 and 3 ms after the voltage step to −100 mV. Both in control and in A9C the corresponding values of steady state currents at −100 mV were subtracted from the above values. Fig. 3C shows that maximal tail current amplitudes in A9C became large than control as prepulse voltages were more depolarized.

In the presence of A9C, tail current decays had complex kinetics that could not always be fit by one or two exponentials, we therefore measured the decay time necessary to reach 50% of the maximal tail current (Fig. 3B, dotted blue line) recorded at −100 mV. Fig. 3D shows that, as expected, t_{50} did not change with voltage in control, as it represents the channels' closure at −100 mV, whereas t_{50} increased with voltage in 1 mM A9C.

These results show that both tail current potentiation and t_{50} increased with depolarization of the prepulse voltage.

3.3. Concentration dependence of A9C effects

Fig. 4A shows representative whole-cell recordings at 1.5 μM Ca^{2+} in control and in the presence of various concentrations of A9C from 33 μM to 1 mM. All the effects of A9C, block, potentiation and change in kinetics were reversible, as shown by the washout traces in the right column of Fig. 4A. I–V relations measured at the end of voltage steps are shown in Fig. 4B. Average fractional currents, I_{A9C}/I_{CT}, plotted as a function of voltage show the presence of a voltage-dependent block at every A9C

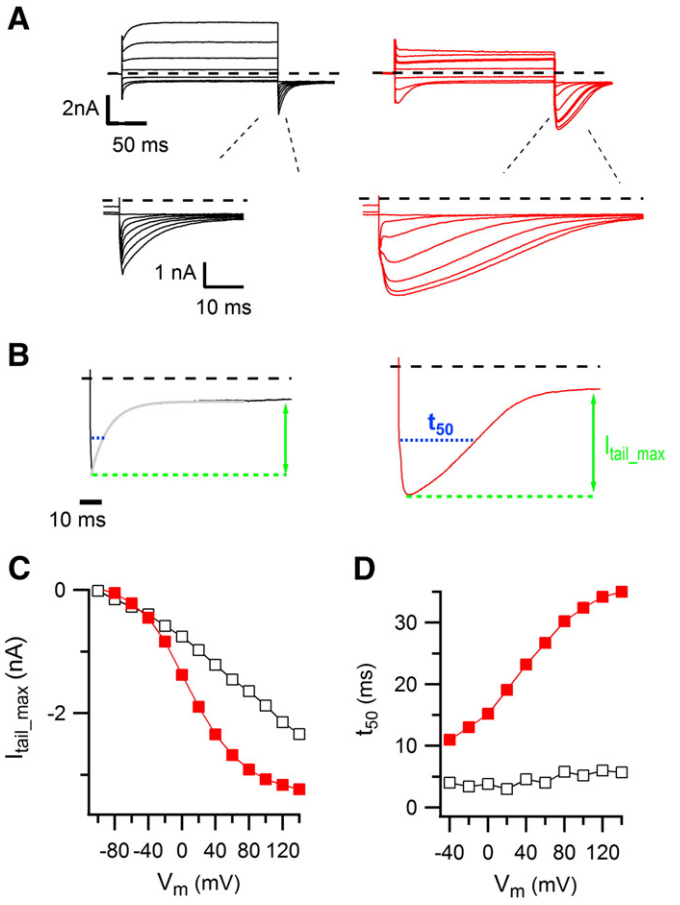

Fig. 3. Multiple effects of A9C. (A) Current recordings in the presence of 1.5 μM intracellular Ca^{2+}, from the same cell in Fig. 2, with voltage steps from −100 to +140 mV from a holding potential of 0 mV in control (black) or in the presence of 1 mM A9C (red). Only recordings every 40 mV are shown. (B) Tail current decay shown in enlarged scale. To evaluate potentiation and slowing of current decay, maximal tail current amplitudes and time of 50% current decay, t_{50}, were calculated with respect to steady-state current at −100 mV. (C) Maximal tail currents, I_{tail_max}, plotted versus membrane potential in control and in 1 mM A9C for the experiment shown in A. Continuous lines represent data interpolation. (D) Time of 50% current decay, t_{50}, versus membrane potential for the experiment shown in A.

concentration (Fig. 4C; n = 4–8 for each concentration). However, Fig. 4B (inset) and C illustrates that in 300 μM A9C there was also a small potentiation ($I_{A9C}/I_{CT} > 1$) of outward currents at voltages between +20 and +60 mV. On average, I_{A9C}/I_{CT} at +40 mV was 1.22 ± 0.07 (n = 6, $p < 0.05$).

As the presence of potentiation prevents a correct evaluation of the blocking potency of A9C at every voltage, we made a rough evaluation of the concentration-dependent block between +80 and +140 mV without taking into account values at 300 μM A9C, because potentiation obscured the blocking effect especially at this concentration. Fig. 5A shows the fractional current I_{A9C}/I_{CT} plotted versus A9C concentration at various voltages. The continuous lines correspond to the fit according to the following equation:

$$I_{A9C}/I_{CT} = 1/(1 + [A9C]/K_D) \quad (1)$$

where K_D is the concentration of A9C producing 50% of the control current at a given voltage.

K_D as a function of membrane potential is plotted in Fig. 5B together with the fit to the Woodhull equation [57,58]:

$$\log K_D(V_m) = \log K_D(0\ mV) + z\delta V_m F/2.3 * RT \quad (2)$$

where V_m is the voltage, z is the electrical charge of the blocker, δ is the fraction of the voltage field sensed by the blocker from the extracellular side, F is the Faraday constant, R is the gas constant, and T is the absolute temperature.

From the best fit of the Woodhull equation to the data (Fig. 5B), with $z = -1$ for A9C, we obtained δ = 0.57 and K_D (0 mV) = 4450 μM.

We quantified the potentiation of tail currents and the deactivation kinetics at −100 mV at various A9C concentrations as previously described in Fig. 3. Fig. 6A and B show respectively the maximal tail currents and t_{50} measured at −100 mV after a prepulse to +120 mV as a function of A9C concentration.

These results show that tail current potentiation had a biphasic dependence on A9C concentration, reaching a maximum amplitude at 300 μM A9C and then decreasing as A9C further increased (Fig. 6A), while t_{50} monotonically increased with A9C concentration (Fig. 6B).

3.4. Effects of A9M, a non-charged analogue of A9C

To test the role of the negative charge of A9C, we used anthracene-9-methanol (A9M), a non-charged analogue of A9C and compared the effect of A9C and A9M at 300 μM. Fig. 7A and B show that A9M had a very small blocking effect on outward currents and did not cause potentiation of inward currents. In the same cell, 300 μM A9C had the typical voltage-dependent effect, blocking outward currents at high depolarizing voltages (Fig. 7A–C) and potentiated early inward currents and tail currents at −100 mV, in agreement with Figs. 4 and 6, while potentiation was not present in 300 μM A9M.

Fig. 7C shows that the small block by A9M was not voltage-dependent (n = 4, the broken line refers to the experiment in panel A). Moreover, the blocking effect of 300 μM A9M was smaller than that of A9C at high depolarizing voltages ($V_m > +60$ mV), similar at about +60 mV, and higher than that of A9C at low positive voltages ($+20 < V_m < +40$ mV), which is the voltage range in which we observed potentiation by 300 μM A9C (Fig. 4C). Thus, the blocking effect by A9C may be underestimated at low positive voltages because of a simultaneous potentiating effect.

In addition, Fig. 7D shows that A9M slowed activation kinetics. On average, τ_{act} at +120 mV in control was 7.55 ± 0.17 ms, whereas it became slower, 18.9 ± 2.1 ms, in the presence of 300 μM A9M (n = 7, $p < 0.05$). Similar values were obtained at voltages between +20 and +140 mV, with τ_{act} about 2.5 fold larger than in control (Fig. 7D). Thus, A9M weakly blocked TMEM16B currents recorded in the presence of 1.5 μM Ca^{2+}, and produced a strong and reversible prolongation of the activation kinetics (Fig. 7A, D).

We also compared the effect of A9M and A9C on the tail currents measured at −100 mV after prepulse voltages from −100 to +140 mV. Fig. 8A shows tail currents from the same experiment of Fig. 7A on an expanded time scale. A9C greatly potentiated tail current amplitude and slowed deactivation as previously shown, while A9M caused a small block of tail current amplitude and a prolongation of the deactivation kinetics, which could be fitted by a single exponential function as in control (Fig. 8B and C).

Taken together, these results show that 300 μM A9M produced a small, not voltage-dependent block of outward currents, did not potentiate tail currents, but prolonged both the activation and deactivation kinetics of TMEM16B.

4. Discussion

Here, we have provided the first study characterizing the effect of extracellular A9C and of its non-charged analogue A9M on the TMEM16B channel. In addition, to the best of our knowledge, this is the first report investigating the action of A9M on a CaCC. Our results, together with future studies aimed at the identification of the specific regions responsible for these effects, will contribute to the elucidation

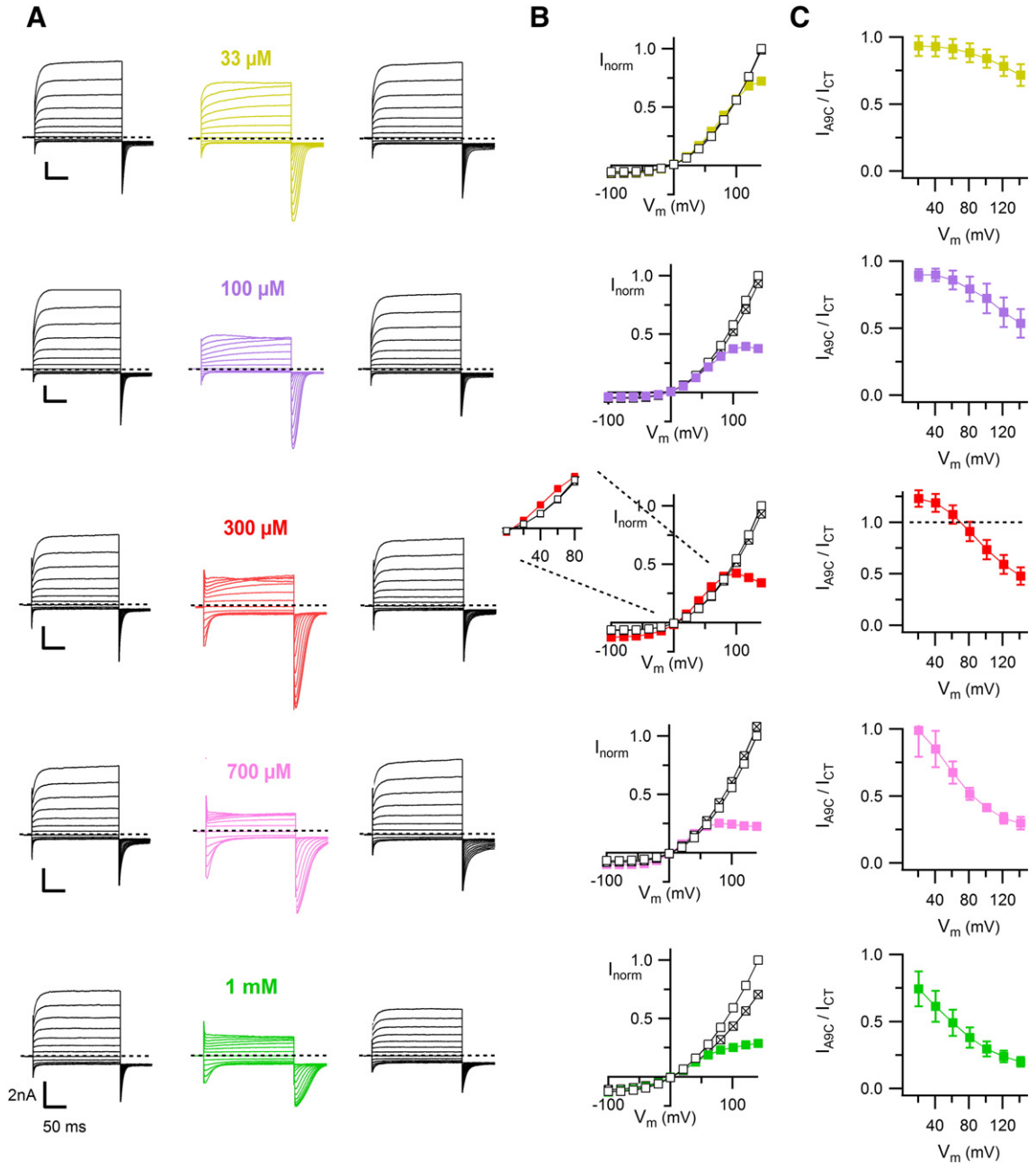

Fig. 4. Concentration dependence of A9C effects. (A) Representative whole-cell recordings in 1.5 μM intracellular Ca^{2+}. Voltage protocol as in Fig. 1. Each cell was exposed to control (black traces on the left), to the indicated concentration of A9C, followed by washout (black traces on the right). (B) I–V relations measured at the end of the voltage steps from the cells shown in A in control (empty square), A9C (filled squares), or after washout (cross squares). Currents were normalized to the value in control at 140 mV. The inset shows the IV on expanded scale for the cell exposed to 300 μM A9C and the potentiating effect of the compound on the current. (C) Average fractional current (I_{A9C}/I_{CT}) as a function of voltage (mean ± SEM n = 4–8 for each A9C concentration).

of the structure, functional properties and action mechanisms of TMEM16B channels.

4.1. Blockage

We found that extracellular A9C produced a voltage-dependent block of TMEM16B-induced outward currents with a stronger block of A9C at high depolarizing potentials, indicating that A9C may bind to a site in the pore inhibiting the flow of permeant anions, whereas A9M, a non-charged analogue of A9C, produced a small, not voltage-dependent block of outward current, probably binding to a site outside the electrical field.

By fitting data obtained with various concentrations of A9C with the Woodhull equation, we estimated that A9C experienced about 57% of the voltage field calculated from the extracellular side and that K_D (0 mV) was about 4450 μM.

Previous studies on endogenous CaCCs have found a voltage-dependent blocking effect of A9C in several cell types ([37,44] in smooth muscle cells from rabbit portal vein; [51] in *Xenopus* oocytes). Moreover, some authors also estimated the A9C concentration inhibiting 50% of the control current (K_D) at different voltages and the location of the blocking site in the voltage field. Qu and Hartzell [51] analyzed A9C block on CaCCs in *X. laevis* oocytes and found that the blocker was sensitive to 60% of the voltage field, similar to our result of 57%. However, they estimated that, at +100 mV (0 mV), the K_D value for A9C was

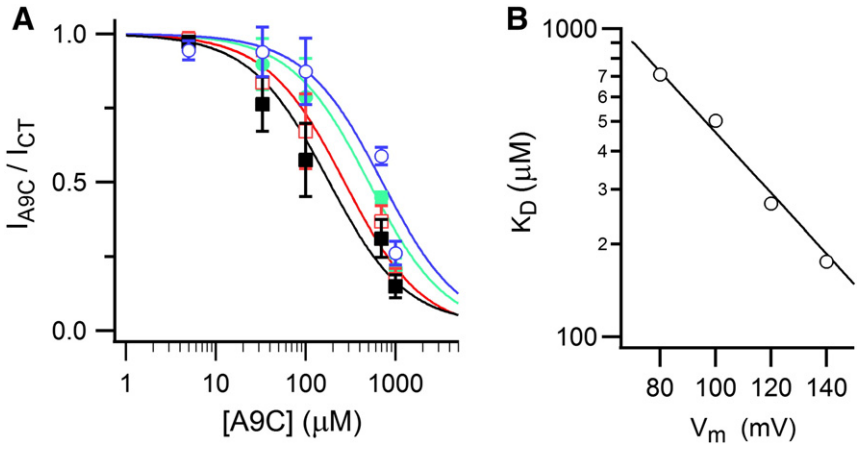

Fig. 5. Concentration dependence of A9C block. (A) Concentration dependence of fractional current (I_{A9C}/I_{CT}) recorded at +140 (black squares), +120 (red empty squares), +100 (green circles), and +80 mV (blue empty circles) in cells recorded in 1.5 μM Ca^{2+} (mean ± SEM; n = 4–8 for each A9C concentration). Continuous lines are the best fit according to Eq. (1) with K_D of 176, 270, 502 and 711 μM respectively at +140, +120, +100, +80 mV. (B) The continuous line is the best fit with the Woodhull Eq. (2) with δ = 0.57, K_D (0 mV) = 4450 μM.

18.3 μM (158 μM), while we obtained the larger values of 502 μM (4450 μM) for TMEM16B (Fig. 5A). This difference can be due to the fact that CaCC in *X. laevis* oocyte is generated by TMEM16A [15], that might be more sensitive to A9C. Indeed, Bradley et al. [59] recently investigated A9C block of hTMEM16A-*acd* mediated currents in HEK293 transfected cells and found K_D = 56 μM for A9C at +80 mV, a value similar to that reported for CaCCs from rabbit portal vein [37,50]. Although these reports seem to indicate that A9C has a higher apparent affinity for TMEM16A than for TMEM16B, [50] estimated that the K_D for A9C was between 700 and 1000 μM for TMEM16A cloned from mouse submandibular glands (Fig. 2D in [50]). Thus, further studies are needed to determine the effect of A9C on different TMEM16A and TMEM16B isoforms and elucidate the molecular mechanisms underlying the different results.

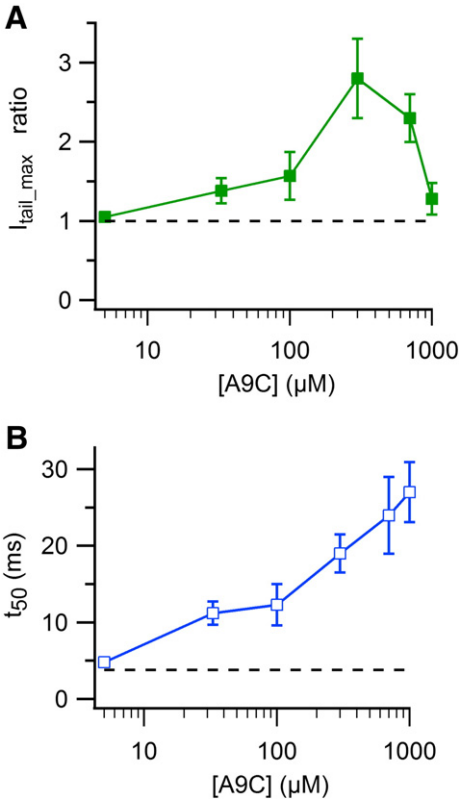

Fig. 6. Concentration dependence of A9C tail current potentiation and prolongation of deactivation kinetics, evaluated as described in Fig. 3B. (A) Average ratios between maximal tail currents, I_{tail_max}, in A9C and control and (B) time of 50% current decay, t_{50}, evaluated at −100 mV, after a prepulse to +120 mV, plotted as a function of A9C concentration (mean ± SEM n = 4–8 for each A9C concentration). Broken line in A and B represents respectively I_{tail_max} and t_{50} in control. The values of t_{50} at each A9C concentration, except for 5 μM, are statistically different from control (ANOVA and post-hoc Tukey's test, $p < 0.05$).

Nonetheless, since the voltage dependence of the block is commonly interpreted to reflect binding of the blocker to a site in the permeation pathway, the similar δ values of about 0.6 found both in our study and by Qu and Hartzell [51], indicate that A9C may bind to a similar location in the pore of TMEM16A and TMEM16B.

Since A9C and A9M are hydrophobic molecules (although A9C also has a negative charge), it is possible that they traverse the membrane bilayer and block from the intracellular side. Qu and Hartzell [51], showed that block of CaCCs in *X. laevis* oocytes by A9C was much faster and that the apparent affinity of A9C was about 5–6 fold greater in outside-out rather than inside-out patches, showing that the block occurred from the extracellular side of the membrane [51]. In our experimental condition, we observed a fast and reversible block both for A9C and A9M, compatible with the time of complete solution exchange, supporting an action from the extracellular side. Furthermore, by performing experiments with 1 mM A9C added to the intracellular solution in the pipette, we measured TMEM16B currents with properties similar to control that could be blocked by the subsequent application of 1 mM extracellular A9C (data not shown)

4.2. Potentiation

In addition to a voltage-dependent block, A9C also caused potentiation of tail current amplitudes, whereas A9M did not produce an increase in tail current amplitude, showing that the negative charge of A9C is required to produce potentiation.

Furthermore, our data indicate that, in the presence of 1.5 μM Ca^{2+}, potentiation required a previous depolarization. Indeed, 1 mM A9C increased the amplitude of transient inward currents (I_{early} in the Results section, identified by the green line in Fig. 2A) following a holding potential of 0 mV, but not of −60 mV. Furthermore, we showed that the amplitude of tail currents recorded at −100 mV after various prepulse voltages became larger in 1 mM A9C compared to control when the prepulse voltage was more depolarized (Result section 3.2). Although both current block and potentiation of tail current amplitudes require depolarization, the two effects may be caused by different mechanisms. Indeed, tail current potentiation was already present when the prepulse voltage was 0 or +20 mV (Fig. 3C), voltages at which the block was negligible (or perhaps masked by potentiation).

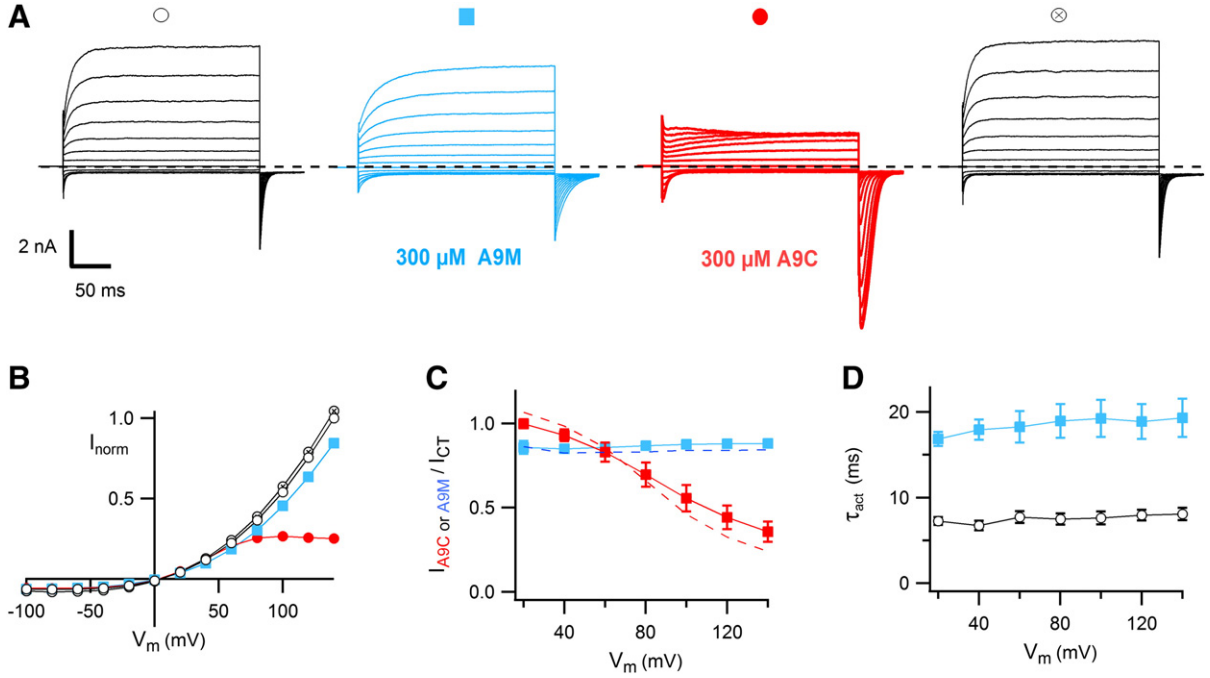

Fig. 7. Effect of A9M, a non-charged analogue of A9C. (A) TMEM16B currents recorded in the presence of 1.5 μM intracellular calcium. The same cell exposed to control solution (black), 300 μM A9M (blue), 300 μM A9C (red) and back to control (black). (B) I–V relations measured at the end of the voltage steps from the cell in A. (C) Comparison of fractional currents (I_{A9C}/I_{CT}) in A9M and control as a function of voltage (n = 5). Broken line refers to the experiment in panel A. (D) Time constant of activation in A9M and control as a function of voltage, showing that application of A9M slowed the activation kinetics (n = 5; paired t-test at each potential, $p < 0.01$).

Moreover, application of low concentrations of A9C, such as 33 μM produced a clear tail current potentiation although the block was small (Figs. 4 and 5A). Also this observation is consistent with the hypothesis that potentiation of tail currents is not caused by the same mechanism responsible for block of outward currents.

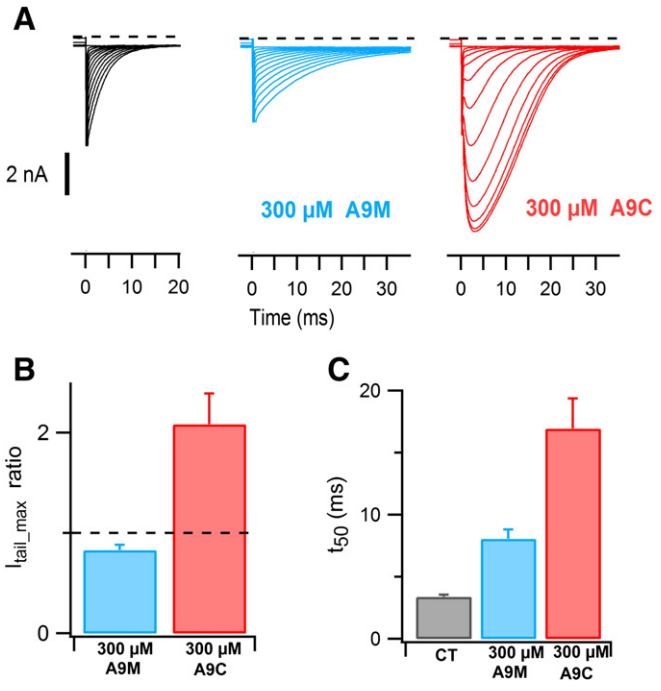

Fig. 8. Comparison of tail currents in A9M and A9C. (A) Tail currents at −100 mV from the same cell in Fig. 7A, shown on an expanded time scale. Currents were recorded in the presence of 1.5 μM intracellular calcium in control bath, 300 μM A9M and A9C. (B) Ratio with respect to control of maximal current amplitudes in the presence of 300 μM A9M or A9C, recorded at −100 mV from a prepulse of +120 mV. Broken line refers to control (n = 5; ANOVA and post-hoc Tukey's test $p < 0.01$). (C) Time of 50% current decay, t_{50}, in control (CT), 300 μM A9C and 300 μM A9M (n = 5; ANOVA and post-hoc Tukey's test $p < 0.05$ between control and A9M, control and A9C, A9M and A9C).

Interestingly, potentiation of tail current amplitudes had a biphasic dependence on A9C concentration (Figs. 4 and 6A), reaching a 3-fold increase at 300 μM, whereas block of outward currents further increased with A9C concentration, further indicating that potentiation and block effects may not be correlated.

Moreover, potentiation of tail currents at −100 mV was accompanied by a marked slowing of channels' closure (Fig. 3). The prolongation of tail current deactivation at −100 mV increased with depolarization of the prepulse potential (Fig. 3D) and, at a given voltage, increased monotonically with A9C concentration (Figs. 4 and 6B).

In the presence of A9C, an initial rising phase was clearly visible in the tail current recorded at −100 mV (Fig. 3). This feature is usually observed in the presence of open channel blockers that have to unbind before channel closure [57,60–62].

At all potentials the uncharged analogue A9M slowed the kinetics of both current activation and deactivation, although the kinetics was simpler with respect to A9C and not accompanied by potentiation.

An anomalous effect of A9C on endogenous CaCCs was reported by Piper and Greenwood [52] in rabbit pulmonary artery smooth muscle cells. Application of 500 μM A9C produced a small inhibition of the maximum outward current at +70 mV, but augmented the amplitude of the instantaneous inward relaxation at −80 mV from an average of −122 pA to −461 pA (about 3.8 fold, Fig. 1B and C in [52]). The same authors also reported the appearance of an initial growth phase in the tail current at −80 mV in the presence of A9C (inset in Fig. 1B in [52]). Moreover, Piper and Greenwood [52] did not observe a significant slowing of the deactivation kinetics at −80 mV.

In a recent study, Bradley et al. [59] also reported a potentiation of A9C on tail currents and a prolongation of tail currents' deactivation of hTMEM16A-*acd* channels, in addition to the voltage-dependent block of outward currents (Figs. 1 and 2 in [59]). However, the kinetics of tail currents was rather different between TMEM16A and TMEM16B. In TMEM16A tail currents decayed mono-exponentially both in control and in the presence of A9C [59], whereas in TMEM16B, A9C produced a

complex kinetics with a decay that could not be fitted with one or two exponentials.

A9C is a well-known blocker not only of CaCCs, but also of diverse Cl conductances such as CFTR and CLC-1 [63–65], although the proteins underlying these currents are not structurally related. It is of interest to note that A9C acts from the intracellular side on CFTR-mediated currents, producing both voltage-dependent block and potentiation [63–66]. In addition, the non-charged A9M fails to block CFTR-induced currents, whereas it still causes potentiation, indicating that in CFTR the negative charge is only involved in the voltage-dependent block but not in the potentiation effects [66].

4.3. Mechanisms for the multiple effects of A9C on TMEM16B

We analyzed possible mechanisms that may be responsible for the block and potentiation effects of A9C on TMEM16B-induced currents. We first considered the possibility that A9C could be an open channel blocker acting with a "foot-in-the-door" mechanism, which prevents channel closure [57,67]. In the presence of 1.5 μM Ca^{2+}, a voltage step to +100 mV causes the opening of about 50% of the channels in control conditions (Fig. 4A in [55]), and a subsequent voltage step to −100 mV produces a tail current which declines with channels' closure (Fig. 5C in [55]). If A9C acts with a "foot-in-the-door" mechanism, channels will be in at least three different states: open, closed or blocked and, as channels reach equilibrium, more than 50% of the channels will be open or blocked. When the voltage is stepped to −100 mV in the presence of A9C, the release of open channel block will occur producing a potentiation of tail current amplitude and a slowing of deactivation compared to control. However, this mechanism cannot explain all our data, as for example we observed that a large potentiation of tail current amplitude at −100 mV was already present at low concentrations of A9C, when the block was very small.

Another possible mechanism responsible for the multiple effects of A9C involves the presence of at least two binding sites for A9C: a site within the channel pore mediating the voltage-dependent open channel block, and a distinct site responsible for potentiation. Although the presence of two binding sites for A9C is consistent with our data, our results are not demonstrative of this hypothesis and we cannot exclude other mechanisms.

5. Conclusions

In conclusion, in this paper we described for the first time the interaction of the traditional CaCC blocker A9C and its non-charged analogue A9M with TMEM16B. A9C inhibited TMEM16B currents at positive voltages, while it enhanced tail currents at negative potentials and strongly prolonged channel closure. A9M caused a weak voltage-independent block of TMEM16B currents, modified current kinetics, but was not effective in potentiating tail currents.

Further studies are needed to understand the complex effects of A9C on TMEM16B channels, as well as on TMEM16A channels, and to identify the molecular mechanisms and the channel's regions responsible for potentiation and block.

Transparency document

The Transparency document associated with this article can be found, in the online version.

Acknowledgements

We thank all members of the laboratory at SISSA and colleagues at IBF for scientific discussion. We thank S. Pifferi for sharing analysis procedures. This study was supported by a grant from the Italian Ministry of Education, University and Research (MIUR, 2010599KBR) and a grant from the Fondazione Compagnia di San Paolo (2013.0922).

References

[1] C.R. Bader, D. Bertrand, E.A. Schwartz, Voltage-activated and calcium-activated currents studied in solitary rod inner segments from the salamander retina, J. Physiol. 331 (1982) 253–284.1.
[2] R. Miledi, A calcium-dependent transient outward current in *Xenopus laevis* oocytes, Proc. R. Soc. Lond. B Biol. Sci. 215 (1982) 491–497.
[3] W.A. Large, Q. Wang, Characteristics and physiological role of the Ca(2+)-activated Cl^- conductance in smooth muscle, Am. J. Physiol. 271 (1996) C435–C454.
[4] S. Frings, D. Reuter, S.J. Kleene, Neuronal Ca^{2+}-activated Cl^- channels—homing in on an elusive channel species, Prog. Neurobiol. 60 (2000) 247–289.
[5] C. Hartzell, I. Putzier, J. Arreola, Calcium-activated chloride channels, Annu. Rev. Physiol. 67 (2005) 719–758.
[6] N. Leblanc, J. Ledoux, S. Saleh, A. Sanguinetti, J. Angermann, K. O'Driscoll, F. Britton, B.A. Perrino, I.A. Greenwood, Regulation of calcium-activated chloride channels in smooth muscle cells: a complex picture is emerging, Can. J. Physiol. Pharmacol. 83 (2005) 541–556.
[7] O.H. Petersen, Ca^{2+} signalling and Ca^{2+}-activated ion channels in exocrine acinar cells, Cell Calcium 38 (2005) 171–200.
[8] S. Wray, T. Burdyga, K. Noble, Calcium signalling in smooth muscle, Cell Calcium 38 (2005) 397–407.
[9] M.R. Lalonde, M.E. Kelly, S. Barnes, Calcium-activated chloride channels in the retina, Channels Austin Tex. 2 (2008) 252–260.
[10] C. Duran, C.H. Thompson, Q. Xiao, H.C. Hartzell, Chloride channels: often enigmatic, rarely predictable, Annu. Rev. Physiol. 72 (2010) 95–121.
[11] J. Berg, H. Yang, L.Y. Jan, Ca^{2+}-activated Cl^- channels at a glance, J. Cell Sci. 125 (2012) 1367–1371.
[12] F. Huang, X. Wong, L.Y. Jan, International Union of Basic and Clinical Pharmacology LXXXV: calcium-activated chloride channels, Pharmacol. Rev. 64 (2012) 1–15.
[13] Y.D. Yang, H. Cho, J.Y. Koo, M.H. Tak, Y. Cho, W.-S. Shim, S.P. Park, J. Lee, B. Lee, B.-M. Kim, R. Raouf, Y.K. Shin, U. Oh, TMEM16A confers receptor-activated calcium-dependent chloride conductance, Nature 455 (2008) 1210–1215.
[14] A. Caputo, E. Caci, L. Ferrera, N. Pedemonte, C. Barsanti, E. Sondo, U. Pfeffer, R. Ravazzolo, O. Zegarra-Moran, L.J.V. Galietta, TMEM16A, a membrane protein associated with calcium-dependent chloride channel activity, Science 322 (2008) 590–594.
[15] B.C. Schroeder, T. Cheng, Y.N. Jan, L.Y. Jan, Expression cloning of TMEM16A as a calcium-activated chloride channel subunit, Cell 134 (2008) 1019–1029.
[16] S. Pifferi, M. Dibattista, A. Menini, TMEM16B induces chloride currents activated by calcium in mammalian cells, Pflugers Arch. - Eur. J. Physiol. 458 (2009) 1023–1038.
[17] A.B. Stephan, E.Y. Shum, S. Hirsh, K.D. Cygnar, J. Reisert, H. Zhao, ANO2 is the cilial calcium-activated chloride channel that may mediate olfactory amplification, Proc. Natl. Acad. Sci. U. S. A. 106 (2009) 11776–11781.
[18] H. Stöhr, J.B. Heisig, P.M. Benz, S. Schöberl, V.M. Milenkovic, O. Strauss, W.M. Aartsen, J. Wijnholds, B.H.F. Weber, H.L. Schulz, TMEM16B, a novel protein with calcium-dependent chloride channel activity, associates with a presynaptic protein complex in photoreceptor terminals, J. Neurosci. Off. J. Soc. Neurosci. 29 (2009) 6809–6818.
[19] C. Sagheddu, A. Boccaccio, M. Dibattista, G. Montani, R. Tirindelli, A. Menini, Calcium concentration jumps reveal dynamic ion selectivity of calcium-activated chloride currents in mouse olfactory sensory neurons and TMEM16b-transfected HEK 293T cells, J. Physiol. 588 (2010) 4189–4204.
[20] M. Dibattista, A. Amjad, D.K. Maurya, C. Sagheddu, G. Montani, R. Tirindelli, A. Menini, Calcium-activated chloride channels in the apical region of mouse vomeronasal sensory neurons, J. Gen. Physiol. 140 (2012) 3–15.
[21] N. Pedemonte, L.J.V. Galietta, Structure and function of TMEM16 proteins (anoctamins), Physiol. Rev. 94 (2014) 419–459.
[22] F. Huang, J.R. Rock, B.D. Harfe, T. Cheng, X. Huang, Y.N. Jan, L.Y. Jan, Studies on expression and function of the TMEM16A calcium-activated chloride channel, Proc. Natl. Acad. Sci. 106 (2009) 21413–21418.
[23] L. Ferrera, A. Caputo, L.J.V. Galietta, TMEM16A protein: a new identity for Ca^{2+}-dependent Cl^- channels, Physiology 25 (2010) 357–363.
[24] J.R. Rock, B.D. Harfe, Expression of TMEM16 paralogs during murine embryogenesis, Dev. Dyn. Off. Publ. Am. Assoc. Anat. 237 (2008) 2566–2574.
[25] G.M. Billig, B. Pál, P. Fidzinski, T.J. Jentsch, Ca^{2+}-activated Cl^- currents are dispensable for olfaction, Nat. Neurosci. 14 (2011) 763–769.
[26] C.A. Flores, L.P. Cid, F.V. Sepúlveda, M.I. Niemeyer, TMEM16 proteins: the long awaited calcium-activated chloride channels? Braz. J. Med. Biol. Res. 42 (2009) 993–1001.
[27] L.J.V. Galietta, The TMEM16 protein family: a new class of chloride channels? Biophys. J. 97 (2009) 3047–3053.
[28] K. Kunzelmann, R. Schreiber, A. Kmit, W. Jantarajit, J.R. Martins, D. Faria, P. Kongsuphol, J. Ousingsawat, Y. Tian, Expression and function of epithelial anoctamins, Exp. Physiol. 97 (2012) 184–192.
[29] K. Kunzelmann, Y. Tian, J.R. Martins, D. Faria, P. Kongsuphol, J. Ousingsawat, L. Wolf, R. Schreiber, Airway epithelial cells—functional links between CFTR and anoctamin dependent Cl^- secretion, Int. J. Biochem. Cell Biol. 44 (2012) 1897–1900.
[30] S. Pifferi, V. Cenedese, A. Menini, Anoctamin 2/TMEM16B: a calcium-activated chloride channel in olfactory transduction, Exp. Physiol. 97 (2012) 193–199.
[31] K.M. Sanders, M.H. Zhu, F. Britton, S.D. Koh, S.M. Ward, Anoctamins and gastrointestinal smooth muscle excitability, Exp. Physiol. 97 (2012) 200–206.
[32] P. Scudieri, E. Sondo, L. Ferrera, L.J.V. Galietta, The anoctamin family: TMEM16A and TMEM16B as calcium-activated chloride channels, Exp. Physiol. 97 (2012) 177–183.
[33] P. Scudieri, E. Sondo, E. Caci, R. Ravazzolo, L.J.V. Galietta, TMEM16A–TMEM16B chimaeras to investigate the structure–function relationship of calcium-activated chloride channels, Biochem. J. 452 (2013) 443–455.

[34] M.M. White, M. Aylwin, Niflumic and flufenamic acids are potent reversible blockers of Ca2(+)-activated Cl^- channels in *Xenopus* oocytes, Mol. Pharmacol. 37 (1990) 720–724.
[35] R.C. Hogg, Q. Wang, W.A. Large, Action of niflumic acid on evoked and spontaneous calcium-activated chloride and potassium currents in smooth muscle cells from rabbit portal vein, Br. J. Pharmacol. 112 (1994) 977–984.
[36] I.A. Greenwood, W.A. Large, Comparison of the effects of fenamates on Ca-activated chloride and potassium currents in rabbit portal vein smooth muscle cells, Br. J. Pharmacol. 116 (1995) 2939–2948.
[37] R.C. Hogg, Q. Wang, W.A. Large, Effects of Cl channel blockers on Ca-activated chloride and potassium currents in smooth muscle cells from rabbit portal vein, Br. J. Pharmacol. 111 (1994) 1333–1341.
[38] Z. Yao, W. Namkung, E.A. Ko, J. Park, L. Tradtrantip, A.S. Verkman, Fractionation of a herbal antidiarrheal medicine reveals eugenol as an inhibitor of Ca^{2+}-activated Cl^- channel TMEM16A, PLoS ONE 7 (2012) e38030.
[39] W. Namkung, J.R. Thiagarajah, P.-W. Phuan, A.S. Verkman, Inhibition of Ca^{2+}-activated Cl^- channels by gallotannins as a possible molecular basis for health benefits of red wine and green tea, FASEB J. 24 (2010) 4178–4186.
[40] F. Huang, H. Zhang, M. Wu, H. Yang, M. Kudo, C.J. Peters, P.G. Woodruff, O.D. Solberg, M.L. Donne, X. Huang, D. Sheppard, J.V. Fahy, P.J. Wolters, B.L.M. Hogan, W.E. Finkbeiner, M. Li, Y.-N. Jan, L.Y. Jan, J.R. Rock, Calcium-activated chloride channel TMEM16A modulates mucin secretion and airway smooth muscle contraction, Proc. Natl. Acad. Sci. U. S. A. 109 (2012) 16354–16359.
[41] R. DeLaFuente, W. Namkung, A. Mills, A.S. Verkman, Small-molecule screen identifies inhibitors of a human intestinal calcium-activated chloride channel, Mol. Pharmacol. 73 (2008) 758–768.
[42] W. Namkung, P.-W. Phuan, A.S. Verkman, TMEM16A inhibitors reveal TMEM16A as a minor component of calcium-activated chloride channel conductance in airway and intestinal epithelial cells, J. Biol. Chem. 286 (2011) 2365–2374.
[43] S.-J. Oh, S.J. Hwang, J. Jung, K. Yu, J. Kim, J.Y. Choi, H.C. Hartzell, E.J. Roh, C.J. Lee, MONNA, a potent and selective blocker for transmembrane protein with unknown function 16/anoctamin-1, Mol. Pharmacol. 84 (2013) 726–735.
[44] R.C. Hogg, Q. Wang, W.A. Large, Time course of spontaneous calcium-activated chloride currents in smooth muscle cells from the rabbit portal vein, J. Physiol. 464 (1993) 15–31.
[45] H.I. Akbarali, W.R. Giles, Ca^{2+} and Ca(2+)-activated Cl^- currents in rabbit oesophageal smooth muscle, J. Physiol. 460 (1993) 117–133.
[46] K.D. Cotton, M.A. Hollywood, N.G. McHale, K.D. Thornbury, Ca^{2+} current and Ca(2+)-activated chloride current in isolated smooth muscle cells of the sheep urethra, J. Physiol. 505 (Pt 1) (1997) 121–131.
[47] C.P. Wayman, I. McFadzean, A. Gibson, J.F. Tucker, Cellular mechanisms underlying carbachol-induced oscillations of calcium-dependent membrane current in smooth muscle cells from mouse anococcygeus, Br. J. Pharmacol. 121 (1997) 1301–1308.
[48] H.M. Toland, K.D. McCloskey, K.D. Thornbury, N.G. McHale, M.A. Hollywood, Ca(2+)-activated Cl(−) current in sheep lymphatic smooth muscle, Am. J. Physiol. Cell Physiol. 279 (2000) C1327–C1335.
[49] Z. Qu, R.W. Wei, H.C. Hartzell, Characterization of Ca^{2+}-activated Cl^- currents in mouse kidney inner medullary collecting duct cells, Am. J. Physiol. Ren. Physiol. 285 (2003) F326–F335.
[50] V.G. Romanenko, M.A. Catalán, D.A. Brown, I. Putzier, H.C. Hartzell, A.D. Marmorstein, M. Gonzalez-Begne, J.R. Rock, B.D. Harfe, J.E. Melvin, TMEM16A encodes the Ca^{2+}-activated Cl^- channel in mouse submandibular salivary gland acinar cells, J. Biol. Chem. 285 (2010) 12990–13001.
[51] Z. Qu, H.C. Hartzell, Functional geometry of the permeation pathway of Ca^{2+}-activated Cl^- channels inferred from analysis of voltage-dependent block, J. Biol. Chem. 276 (2001) 18423–18429.
[52] A.S. Piper, I.A. Greenwood, Anomalous effect of anthracene-9-carboxylic acid on calcium-activated chloride currents in rabbit pulmonary artery smooth muscle cells, Br. J. Pharmacol. 138 (2003) 31–38.
[53] S. Ponissery Saidu, A.B. Stephan, A.K. Talaga, H. Zhao, J. Reisert, Channel properties of the splicing isoforms of the olfactory calcium-activated chloride channel anoctamin 2, J. Gen. Physiol. 141 (2013) 691–703.
[54] C. Patton, S. Thompson, D. Epel, Some precautions in using chelators to buffer metals in biological solutions, Cell Calcium 35 (2004) 427–431.
[55] V. Cenedese, G. Betto, F. Celsi, O.L. Cherian, S. Pifferi, A. Menini, The voltage dependence of the TMEM16B/anoctamin2 calcium-activated chloride channel is modified by mutations in the first putative intracellular loop, J. Gen. Physiol. 139 (2012) 285–294.
[56] G. Betto, O.L. Cherian, S. Pifferi, V. Cenedese, A. Boccaccio, A. Menini, Interactions between permeation and gating in the TMEM16B/anoctamin2 calcium-activated chloride channel, J. Gen. Physiol. 143 (2014) 703–718.
[57] B. Hille, Ion Channels of Excitable Membranes, Third ed. Sinauer Associates, Sunderland, Mass, 2001. (3rd Edition).
[58] A.M. Woodhull, Ionic blockage of sodium channels in nerve, J. Gen. Physiol. 61 (1973) 687–708.
[59] E. Bradley, S. Fedigan, T. Webb, M.A. Hollywood, K.D. Thornbury, N.G. McHale, G.P. Sergeant, Pharmacological characterization of TMEM16A currents, Channels Austin Tex. 8 (2014).
[60] C.M. Armstrong, Time course of TEA(+)-induced anomalous rectification in squid giant axons, J. Gen. Physiol. 50 (1966) 491–503.
[61] C.M. Armstrong, Inactivation of the potassium conductance and related phenomena caused by quaternary ammonium ion injection in squid axons, J. Gen. Physiol. 54 (1969) 553–575.
[62] M.D. Cahalan, W. Almers, Block of sodium conductance and gating current in squid giant axons poisoned with quaternary strychnine, Biophys. J. 27 (1979).
[63] S.S. Zhou, A. Takai, M. Tominaga, Y. Okada, Phosphatase-mediated enhancement of cardiac cAMP-activated Cl^- conductance by a Cl^- channel blocker, anthracene-9-carboxylate, Circ. Res. 81 (1997) 219–228.
[64] D.S. Astill, G. Rychkov, J.D. Clarke, B.P. Hughes, M.L. Roberts, A.H. Bretag, Characteristics of skeletal muscle chloride channel C1C-1 and point mutant R304E expressed in Sf-9 insect cells, Biochim. Biophys. Acta 1280 (1996) 178–186.
[65] K. Steinmeyer, C. Ortland, T.J. Jentsch, Primary structure and functional expression of a developmentally regulated skeletal muscle chloride channel, Nature 354 (1991) 301–304.
[66] T. Ai, S.G. Bompadre, Y. Sohma, X. Wang, M. Li, T.-C. Hwang, Direct effects of 9-anthracene compounds on cystic fibrosis transmembrane conductance regulator gating, Pflugers Arch. - Eur. J. Physiol. 449 (2004) 88–95.
[67] C.M. Armstrong, Interaction of tetraethylammonium ion derivatives with the potassium channels of giant axons, J. Gen. Physiol. 58 (1971) 413–437.